Electronic Supporting Information

Low-temperature Redox Activity and Alcohol Ammoxidation Performance on Cu- and Ru-incorporated Ceria Catalysts

Chaoqi Chen,[a] Satoru Ikemoto,[a] Gen-ichi Yokota,[a] Kimitaka Higuchi,[b] Satoshi Muratsugu,*[a,c] and Mizuki Tada*[a,c,d]

[a] Department of Chemistry, Graduate School of Science, Nagoya University, Furo-cho, Chikusa-ku, Nagoya, Aichi 464-8602, Japan

[b] Institute of Materials and Systems for Sustainability, Nagoya University. Furo-cho, Chikusa-ku, Nagoya, Aichi 464-8602, Japan

[c] Integrated Research Consortium on Chemical Sciences (IRCCS), Nagoya University, Furo-cho, Chikusa-ku, Nagoya, Aichi 464-8602, Japan

[d] Research Center for Materials Science (RCMS), Nagoya University, Furo-cho, Chikusa-ku, Nagoya, Aichi 464-8602, Japan

E-mail: muratsugu.satoshi.a5@f.mail.nagoya-u.ac.jp, tada.mizuki.u6@f.mail.nagoya-u.ac.jp

Contents

Structural characterization of as-prepared $Cu_{0.18}Ru_{0.05}CeO_z$

Table S1. Metal Compositions Estimated by ICP-OES Analysis and BET Surface Areas for N_2 Adsorption for As-prepared $Cu_{0.18}Ru_{0.05}CeO_z$, $Cu_{0.18}CeO_z$, $Ru_{0.04}CeO_z$, and CeO_z

Prepared oxide	BET surface area /m^2 g^{-1}	Molar ratio of Cu/Ru/Ce
$Cu_{0.18}Ru_{0.05}CeO_z$	1.24×10^2	0.178/0.05/1
$Cu_{0.18}CeO_z$	1.05×10^2	0.0176/<0.002/1
$Ru_{0.04}CeO_z$	1.14×10^2	<0.0004/0.040/1
CeO_z	1.20×10^2	-

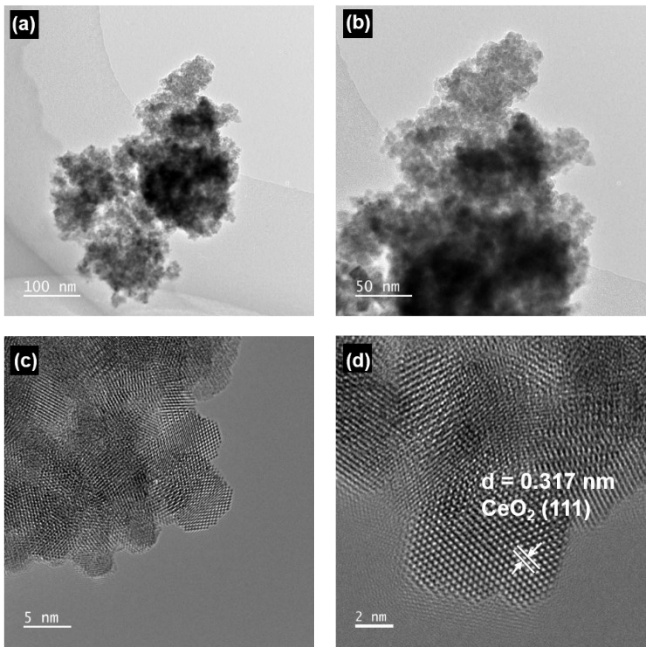

Fig. S1. TEM images of as-prepared $Cu_{0.18}Ru_{0.05}CeO_z$.

Table S2. Ru Oxidation States of As-prepared $Cu_{0.18}Ru_{0.05}CeO_z$ Estimated by Ru K-edge XANES Analysis and References

Ru sample	Energy /eV[a]	Oxidation state
Ru^0 powder	22116.0	0
$Ru(acac)_3$	22120.6	3
RuO_2	22121.3	4
$KRuO_4$	22125.5	7
$Cu_{0.18}Ru_{0.05}CeO_z$ (as-prepared)	22122.2	4.5[b]

[a] The energy at the 50% level of the edge jump in the spectrum. [b] Calculated from the calibration curve in Fig. S2(b).

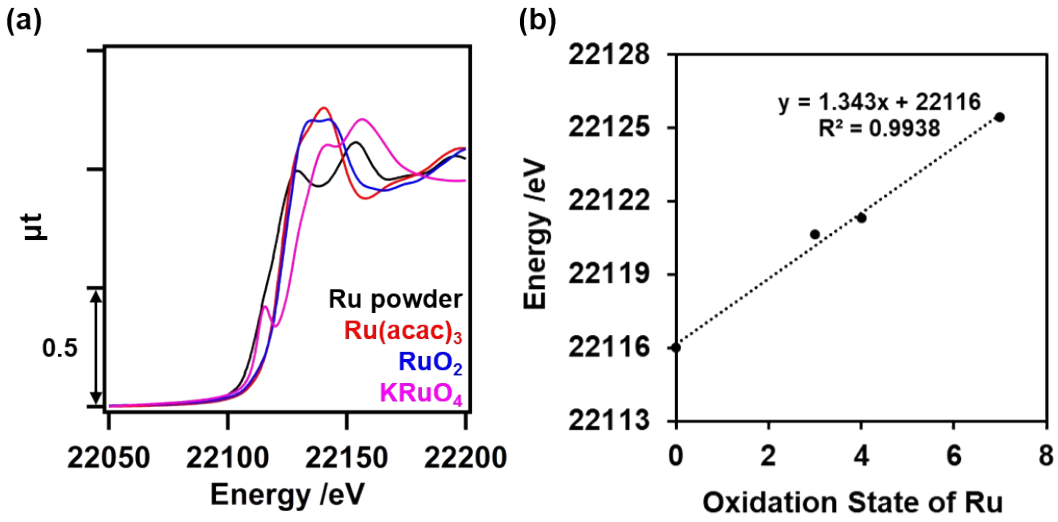

Fig. S2. (a) Ru K-edge XANES spectra of standard samples and (b) calibration curve obtained from the energy at the 50% level of the Ru K-edge jump.

Table S3. Ratio of Ce^{3+} and Ce^{4+} on As-prepared $Cu_{0.18}Ru_{0.05}CeO_z$ Calculated from the Ce 3d XPS Spectrum

Sample	Ratio of Ce^{3+}	Ratio of Ce^{4+}
$Cu_{0.18}Ru_{0.05}CeO_z$ (as-prepared)	0.27	0.73

XPS spectra in Fig. 1(c3) in the main text were used for the calculation. The sum of the areas of u', u_0, v', and v_0, which were attributed to Ce^{3+} (pink line in Fig. 1(c3)),[1] was calculated (area (A)). The sum of the areas of u''', u'', u_0, v''', v'', and v_0, which were attributed to Ce^{4+} (black line in Fig. 1(c3))[1,2], was calculated (area (B)). The ratio of Ce^{3+} or Ce^{4+} was calculated as (area (A) or area (B))/(area (A) + area (B)).

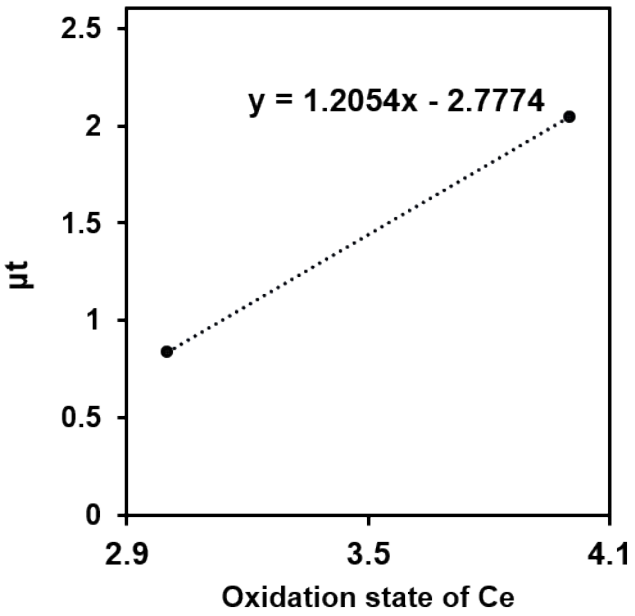

Fig. S3. Calibration curve for Ce L_{III}-edge XANES spectra for the oxidation state calculation of Ce in $Cu_{0.18}Ru_{0.05}CeO_z$. The intensity of the Ce L_{III}-edge at 5741.3 eV (peak top of CeO_2) was used for commercial CeO_2 and $Ce_2(CO_3)_3$ (Ce^{4+} and Ce^{3+} references, respectively).

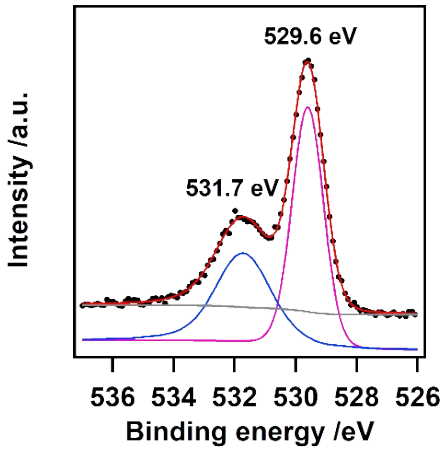

Fig. S4. O 1s XPS spectrum of as-prepared $Cu_{0.18}Ru_{0.05}CeO_z$. The peak at 529.6 eV was attributed to lattice oxygen of CeO_2[3] and that at 531.7 eV was attributed to hydroxyl groups[4] or oxygen vacancies from Ce^{3+} of CeO_2.[5]

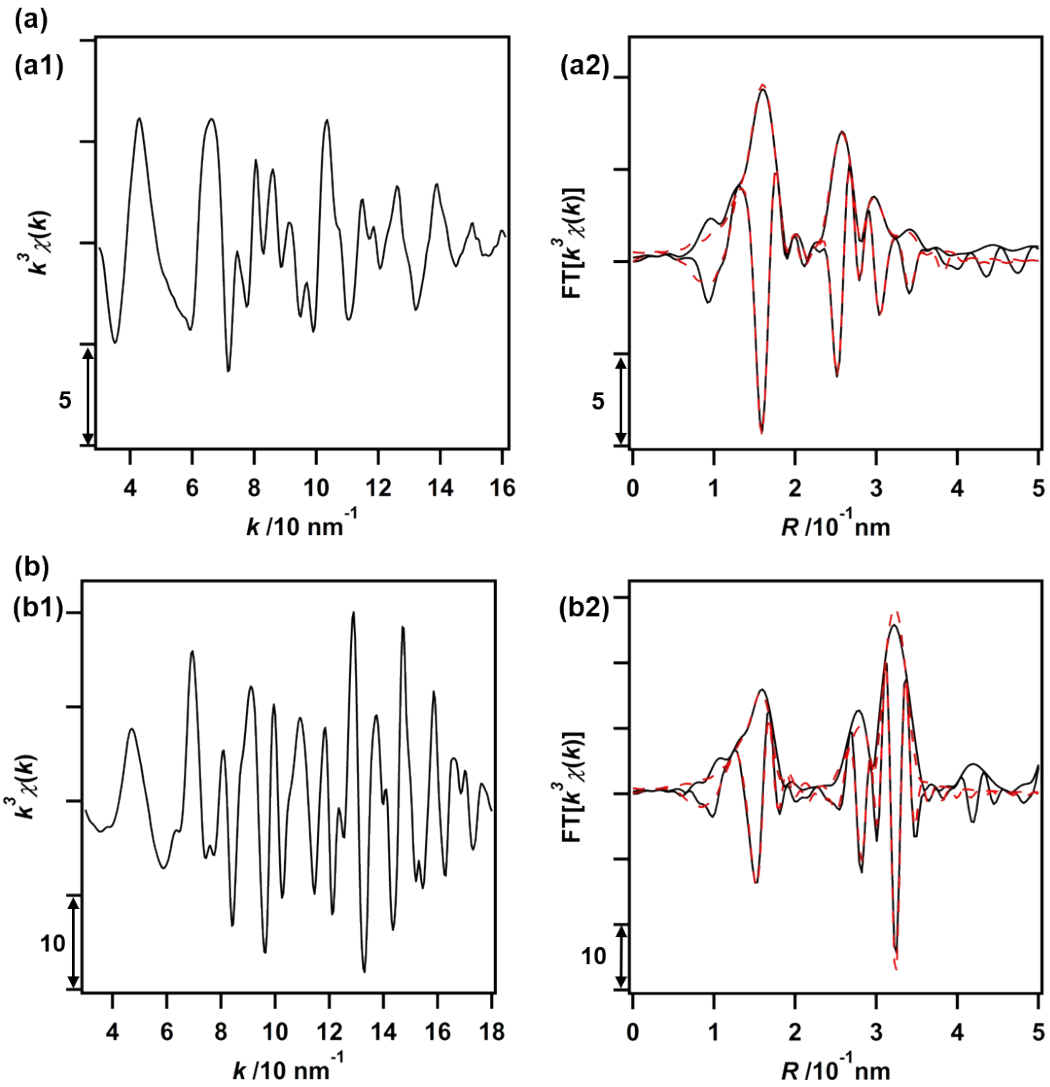

Fig. S5. (a) Cu K-edge EXAFS (a1) oscillation and (a2) Fourier transform for reference CuO (k = 30−160 nm^{-1}). Black solid lines showed observed data and red dashed lines showed fitted data. (b) Ru K-edge EXAFS (b1) oscillation and (b2) Fourier transform for reference RuO_2 (k = 30−180 nm^{-1}). Black solid lines showed observed data and red dashed lines showed fitted data.

Table S4. Structural Parameters Obtained by the Curve-Fitting Analysis of Cu K-edge EXAFS Fourier Transform (Measured at 298 K) of Reference CuO

Path	Shell	CN	R /nm	ΔE /eV	σ^2 /10^{-5} nm^2	R_f %
1	Cu-O	2	0.191 ± 0.001	4.2 ± 0.8	2 ± 1	
2	Cu-O	2	0.200 ± 0.001	4.2 ± 0.8	2 ± 1	
3	Cu-O	2	0.286 ± 0.004	4.2 ± 0.8	2 ± 1	
4	Cu---Cu	4	0.293 ± 0.002	5.6 ± 2.3	8 ± 2	
5	Cu---Cu	4	0.312 ± 0.001	5.6 ± 2.3	8 ± 2	
6	Cu---Cu	2	0.322 ± 0.003	5.6 ± 2.3	8 ± 2	0.6
7	Cu-O	2	0.334 ± 0.007	4.2 ± 0.8	2 ± 1	
8	Cu---Cu	2	0.340 ± 0.003	5.6 ± 2.3	8 ± 2	
9	Cu-O	2	0.348 ± 0.004	4.2 ± 0.8	2 ± 1	
10	Cu---Cu	2	0.383 ± 0.004	5.6 ± 2.3	8 ± 2	
11	Cu-O	2	0.395 ± 0.005	4.2 ± 0.8	2 ± 1	

S_0^2 was calculated to be 0.70 ± 0.05, k = 30–160 nm^{-1}, R = 0.10–0.38 nm. CNs of all shells were fixed.

Table S5. Structural Parameters Obtained by the Curve-Fitting Analysis of Ru K-edge EXAFS Fourier Transform (Measured at 298 K) of Reference RuO_2

Path	Shell	CN	R /nm	ΔE /eV	σ^2 /10^{-5} nm^2	R_f %
1	Ru-O	6	0.197 ± 0.001	7.2 ± 2.0	3 ± 1	
2	Ru---Ru	2	0.312 ± 0.001	7.7 ± 2.4	3 ± 1	
3	Ru-O	4	0.327 ± 0.005	7.2 ± 2.0	3 ± 1	3.0
4	Ru---Ru	8	0.355 ± 0.001	7.7 ± 2.4	3 ± 1	
5	Ru-O	4	0.374 ± 0.007	7.2 ± 2.0	3 ± 1	

S_0^2 was calculated to be 0.86 ± 0.13. k = 30–180 nm^{-1}, R = 0.10–0.38 nm. CNs of all shells were fixed.

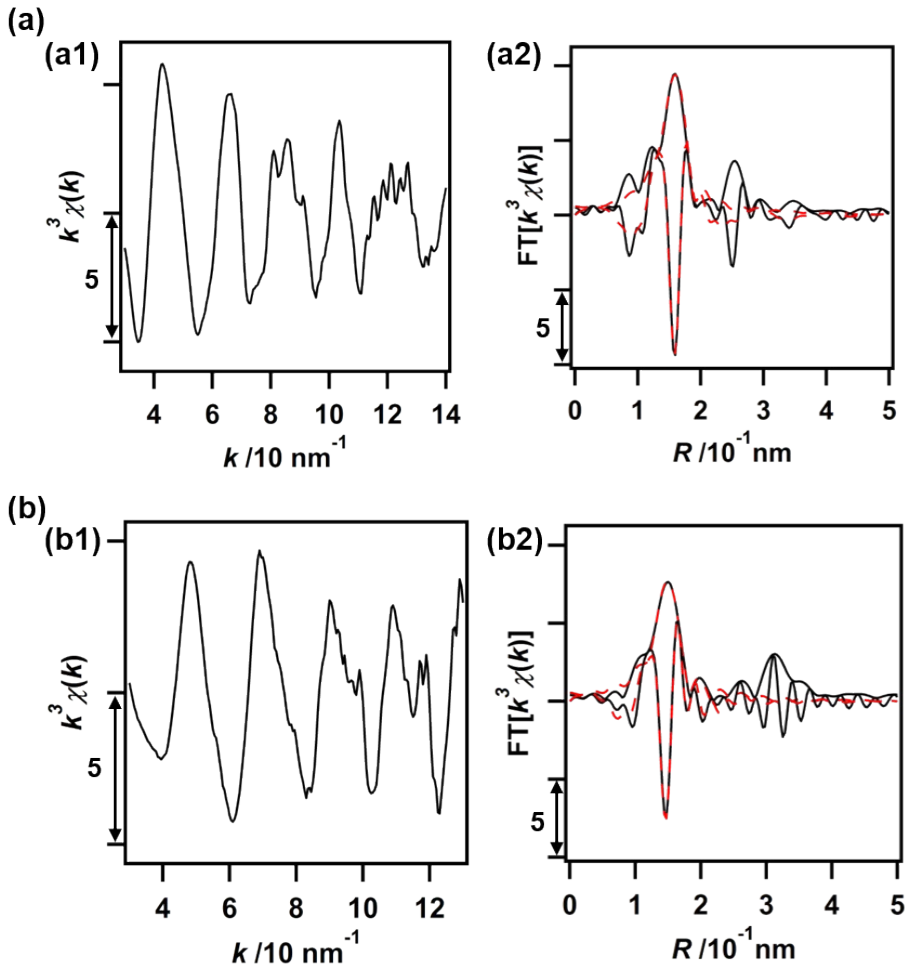

Fig. S6. (a) Cu K-edge EXAFS (a1) oscillation and (a2) Fourier transform for as-prepared $Cu_{0.18}Ru_{0.05}CeO_z$ (k = 30−140 nm^{-1}). (b) Ru K-edge EXAFS (b1) oscillation and (b2) Fourier transform for as-prepared $Cu_{0.18}Ru_{0.05}CeO_z$ (k = 30−130 nm^{-1}). (a2 and b2) Black solid lines showed observed data and red dashed lines showed fitted data.

Table S6. Structural Parameters Obtained by the Curve-Fitting Analysis of Cu K-edge EXAFS Fourier Transform (Measured at 298 K) of As-prepared $Cu_{0.18}Ru_{0.05}CeO_z$

Sample	Shell	CN	R /nm	ΔE /eV	σ^2 /10^{-5} nm^2	R_f /%
$Cu_{0.18}Ru_{0.05}CeO_z$ (as-prepared)	Cu-O	4.6 ± 1.2	0.196 ± 0.002	4.5 ± 3.5	5 ± 3	0.9

S_0^2 was fixed to be 0.70, k = 30–140 nm^{-1}, R = 0.12–0.19 nm.

Table S7. Structural Parameters Obtained by the Curve-Fitting Analysis of Ru K-edge EXAFS Fourier Transform (Measured at 298 K) of As-prepared $Cu_{0.18}Ru_{0.05}CeO_z$

Sample	Shell	CN	R /nm	ΔE /eV	σ^2 /10^{-5} nm^2	R_f /%
$Cu_{0.18}Ru_{0.05}CeO_z$ (as-prepared)	Ru-O	3.2 ± 1.0	0.194 ± 0.002	9.4 ± 4.9	3 ± 2	0.2

S_0^2 was fixed as 0.86, k = 30–130 nm^{-1}, R = 0.12–0.19 nm.

Redox performance evaluation

Table S8. Results of TPR and TPO on $Cu_{0.18}Ru_{0.05}CeO_z$, $Cu_{0.18}CeO_z$, and $Ru_{0.04}CeO_z$

Catalyst	Peak top of H_2-TPR /K	H_2 consumption /mmol $g_{\_cat}^{-1}$ 523 K	O_2 consumption /mmol $g_{\_cat}^{-1}$ 573 K
As-prepared $Cu_{0.18}Ru_{0.05}CeO_z$	353 and 363	2.39	0.92
Second TPR of $Cu_{0.18}Ru_{0.05}CeO_z$	333	1.98	0.93
Third TPR of $Cu_{0.18}Ru_{0.05}CeO_z$	317 – 331	1.90	0.92
Fourth TPR of $Cu_{0.18}Ru_{0.05}CeO_z$	315 – 331	1.96	0.91
Control group I			
As-prepared $Cu_{0.18}CeO_z$	415	1.44	0.89
Second TPR of $Cu_{0.18}CeO_z$	409	1.51	0.89
Third TPR of $Cu_{0.18}CeO_z$	361 and 389	1.47	0.90
Fourth TPR of $Cu_{0.18}CeO_z$	361 and 389	1.49	0.91
As-prepared $Ru_{0.04}CeO_z$	339	1.60	0.88
Second TPR of $Ru_{0.04}CeO_z$	319	1.36	0.87
Third TPR of $Ru_{0.04}CeO_z$	317	1.26	0.87
Fourth TPR of $Ru_{0.04}CeO_z$	317	1.27	0.87
As-prepared CeO_z [2]	673	0.51 (303–773 K)	-
Control group II			
CuO (commercial product from Wako)	477	5.90 (303–773 K)	-
RuO_2 (commercial product from Wako)	429	5.67 (303–773 K)	-

Sample amounts: 200 mg (as-prepared $Cu_{0.18}Ru_{0.05}CeO_z$ and control group I), 14.6 mg (CuO), and 7.1 mg (RuO_2). The sample was treated with 27 kPa H_2 and the temperature was increased at a rate of 5 K min^{-1} from 303 to 523 K, except for CeO_z, CuO, and RuO_2 to 773 K. Then, the sample was treated with 27 kPa O_2 from 303 to 573 K at a rate of 5 K min^{-1} and held at 573 K for 2 h. Once the entire system returned to 293 K, the second and subsequent rounds of TPR and TPO measurements were conducted by introducing 27 kPa H_2 or O_2 gas by a similar procedure. The change in the pressure was recorded at appropriate intervals.

Table S9. Ru Oxidation States of $Cu_{0.18}Ru_{0.05}CeO_z$ After First H_2 Reduction, First O_2 Oxidation, and Second H_2 Reduction Estimated by *In Situ* Ru K-edge XANES Spectra

Standard Ru sample	Energy /eV[a]	Ru oxidation state[b]
$Cu_{0.18}Ru_{0.05}CeO_z$ (after first H_2 reduction)	22117.6	1.06
$Cu_{0.18}Ru_{0.05}CeO_z$ (after first O_2 oxidation)	22122.1	4.40
$Cu_{0.18}Ru_{0.05}CeO_z$ (after second H_2 reduction)	22116.4	0.19

[a] Energy at the 50% level of the absorption edge jump. [b] Calculated from the calibration curve in Fig. S2(b).

Table S10. Linear Combination Fitting of *In Situ* Cu K-edge XANES for $Cu_{0.18}Ru_{0.05}CeO_z$ After First H_2 Reduction, First O_2 Oxidation, and Second H_2 Reduction

Sample	Coefficient c_1 of CuO	Coefficient c_2 of Cu_2O	Coefficient c_3 of Cu	Average oxidation states of Cu[a]
$Cu_{0.18}Ru_{0.05}CeO_z$ (after first H_2 reduction)	0.00	0.30	0.70	0.30
$Cu_{0.18}Ru_{0.05}CeO_z$ (after first O_2 oxidation)	1.00	0.00	0.00	2.00
$Cu_{0.18}Ru_{0.05}CeO_z$ (after second H_2 reduction)	0.00	0.29	0.71	0.29

Fitting equation: spectrum (sample) = c_1 × spectrum (CuO) + c_2 × spectrum (Cu_2O) + c_3 × spectrum (Cu foil). Energy range of the fitting: 8960.3–9010.3 eV. $c_1 + c_2 + c_3$ was fixed as 1.
[a] Average oxidation state of Cu in the sample was calculated from the three coefficients (c_1, c_2, and c_3).

Table S11. Ce Oxidation States of $Cu_{0.18}Ru_{0.05}CeO_z$ After First H_2 Reduction, First O_2 Oxidation, and Second H_2 Reduction Estimated by *In Situ* Ce L_{III}-edge XANES Spectra

Sample	Ce oxidation state[a]
$Cu_{0.18}Ru_{0.05}CeO_z$ (after first H_2 reduction)	3.62
$Cu_{0.18}Ru_{0.05}CeO_z$ (after first O_2 oxidation)	3.83
$Cu_{0.18}Ru_{0.05}CeO_z$ (after second H_2 reduction)	3.62

[a] Calculated from the calibration curve in Fig. S3.

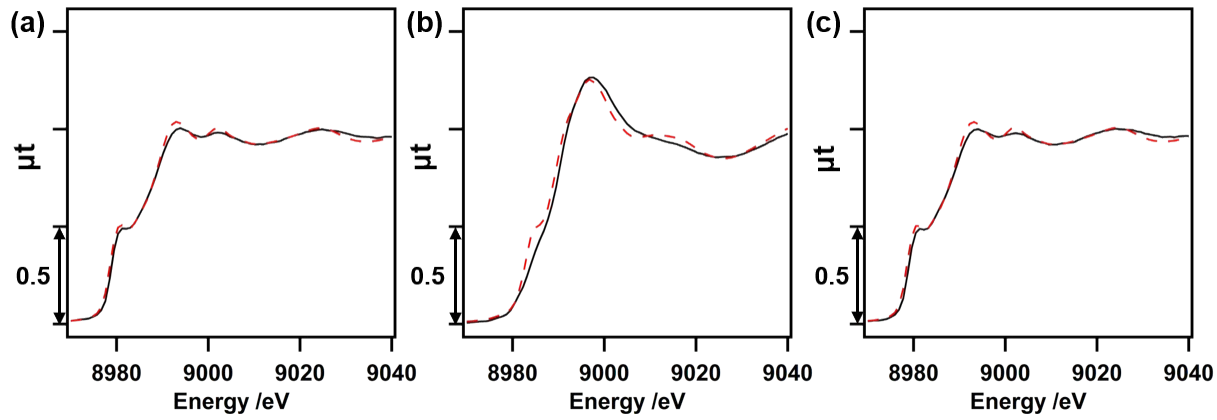

Fig. S7. Cu K-edge *in situ* XANES spectra for $Cu_{0.18}Ru_{0.05}CeO_z$. (a) After first H_2 reduction, (b) after first O_2 oxidation, and (c) after second H_2 reduction. Black lines show the observed spectrum of $Cu_{0.18}Ru_{0.05}CeO_z$ after H_2 or O_2 treatment. Red dashed lines show the LCF fitting spectrum of $Cu_{0.18}Ru_{0.05}CeO_z$ after H_2 or O_2 treatment.

Table S12. Calculated H_2/O_2 Consumptions Corresponding to the Reduction/Oxidation of Metal Species in $Cu_{0.18}Ru_{0.05}CeO_z$ Estimated from the *In Situ* Cu K-edge, Ru K-edge, and Ce L_{III}-edge XANES Spectral Changes [a]

Metal species	H_2 consumption in the first TPR /mmol $g_{\_cat}^{-1}$	O_2 consumption in the first TPO /mmol $g_{\_cat}^{-1}$	H_2 consumption in the second TPR /mmol $g_{\_cat}^{-1}$
Cu	0.78	0.39	0.79
Ru	0.43	0.25	0.49
Ce	0.60	0.21	0.57
Total	1.81	0.85	1.85

[a] Changes in the oxidation states were estimated from the changes in the *in situ* XANES before and after the reduction or oxidation (Fig. 3). The valence changes were calculated as the H_2/O_2 consumption on 1 g of $Cu_{0.18}Ru_{0.05}CeO_z$. Finally, the sum of the consumed H_2/O_2 was calculated as the total.

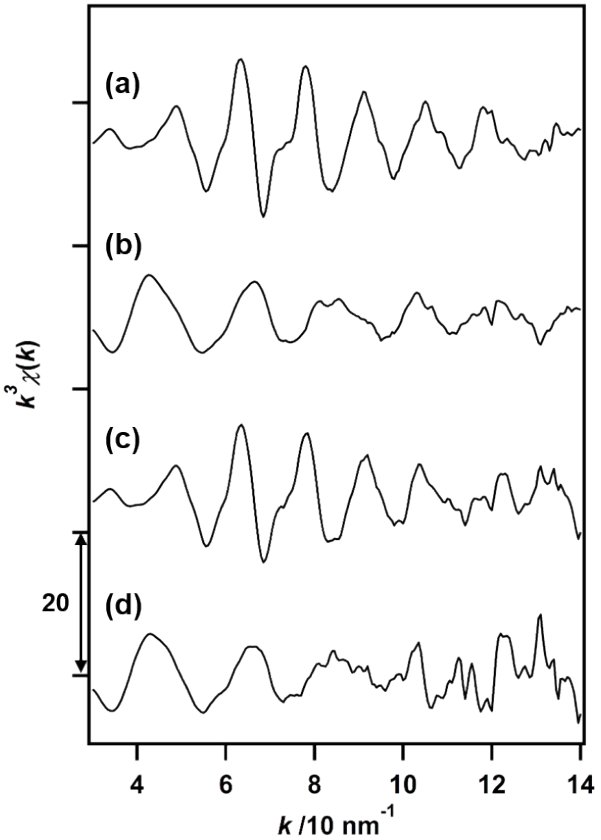

Fig. S8. Cu K-edge EXAFS oscillations for $Cu_{0.18}Ru_{0.05}CeO_z$ (k = 30–140 nm^{-1}). (a) After first H_2 reduction at 523 K, (b) after first O_2 oxidation at 573 K, (c) after third H_2 reduction at 523 K, and (d) after third O_2 oxidation at 573 K.

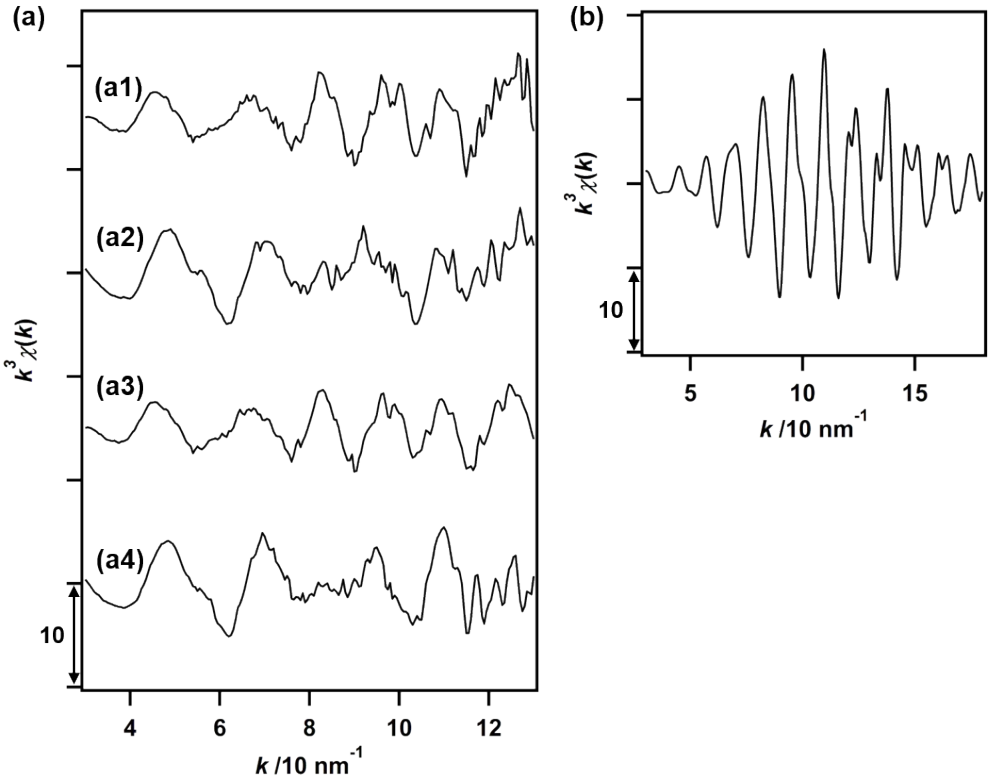

Fig. S9. (a) Ru K-edge EXAFS oscillations for $Cu_{0.18}Ru_{0.05}CeO_z$ (k = 30–130 nm^{-1}). (a1) After first H_2 reduction at 523 K, (a2) after first O_2 oxidation at 573 K, (a3) after third H_2 reduction at 523 K, and (a4) after third O_2 oxidation at 573 K. (b) A Ru K-edge EXAFS oscillation for Ru powder (k = 30–180 nm^{-1}).

Table S13. Structural Parameters Obtained by Curve-Fitting Analysis of Cu K-edge EXAFS Fourier Transforms (Measured at 298 K) for $Cu_{0.18}Ru_{0.05}CeO_z$ After the First and Third Redox Cycles

Sample	Shell	CN	R /nm	ΔE /eV	σ^2 /10^{-5} nm^2	R_f /%
(a1) After first H_2 reduction at 523 K	Cu-Cu	6.1 ± 0.9	0.253 ± 0.001	−0.1 ± 1.4	10 ± 1	0.5
(a2) After first O_2 oxidation at 573 K	Cu-O	4.7 ± 0.8	0.196 ± 0.002	3.9 ± 3.8	5 ± 2	2.0
(a3) After third H_2 reduction at 523 K	Cu-Cu	6.9 ± 1.0	0.252 ± 0.001	−0.9 ± 2.0	12 ± 1	0.8
(a4) After third O_2 oxidation at 573 K	Cu-O	5.7 ± 2.7	0.195 ± 0.004	2.5 ± 6.7	8 ± 5	3.9

S_0^2 was fixed as 1 for metallic Cu and 0.70 for Cu^{2+} oxide. k = 30–140 nm^{-1}, R = 0.18–0.27 nm (a1), 0.12–0.19 nm (a2), 0.18–0.27 nm (a3), and 0.12–0.19 nm (a4).

Ammoxidation performance of $Cu_{0.18}Ru_{0.05}CeO_z$

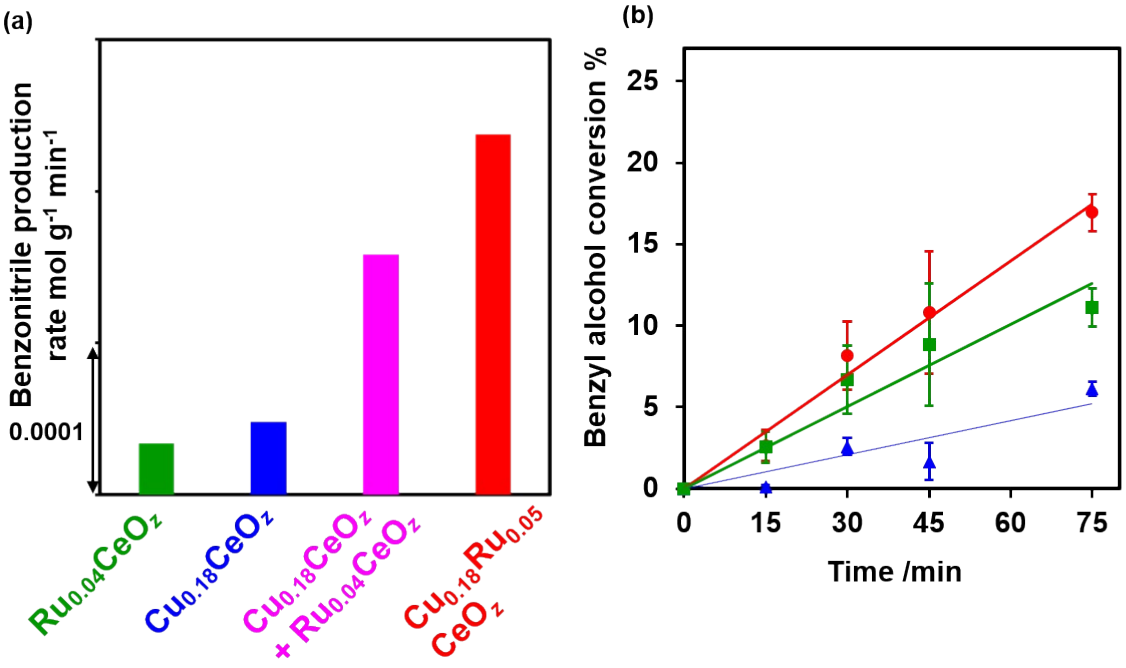

Fig. S10. (a) Benzonitrile production rates for $Cu_{0.18}Ru_{0.05}CeO_z$ (red), $Cu_{0.18}CeO_z$ (blue), $Ru_{0.04}CeO_z$ (green), and a physical mixture of $Cu_{0.18}CeO_z$ and $Ru_{0.04}CeO_z$ (pink). (b) Initial reaction rate of $Cu_{0.18}Ru_{0.05}CeO_z$ (red), $Cu_{0.18}CeO_z$ (blue), and $Ru_{0.04}CeO_z$ (green). The reaction was carried out by using four different autoclaves at 423 K and stopped at 15, 30, 45, and 75 min. Each reaction was performed three times to obtain the error bars. $Cu_{0.18}CeO_z$ + $Ru_{0.04}CeO_z$ was obtained by physically mixing the two catalysts together.

Benzonitrile production rates were calculated by (amount of benzonitrile produced, mmol)/(catalyst weight, g)/(reaction time, min).

Reaction conditions: Benzyl alcohol (1.93 mmol), toluene (1.0 mL), dodecane (internal standard; 0.07 mL), NH_3 (0.32 MPa), O_2 (1.0 MPa), 423 K. Mass balance was over 0.9 at this experiment. $Cu_{0.18}Ru_{0.05}CeO_z$ (14.7 mg), Ru/Cu/alcohol/dodecane = 1/3.5/500/500. $Cu_{0.18}CeO_z$ (14.3 mg), Cu/alcohol/dodecane = 1/150/150. $Ru_{0.04}CeO_z$ (15.3 mg), Ru/alcohol/dodecane = 1/500/500.

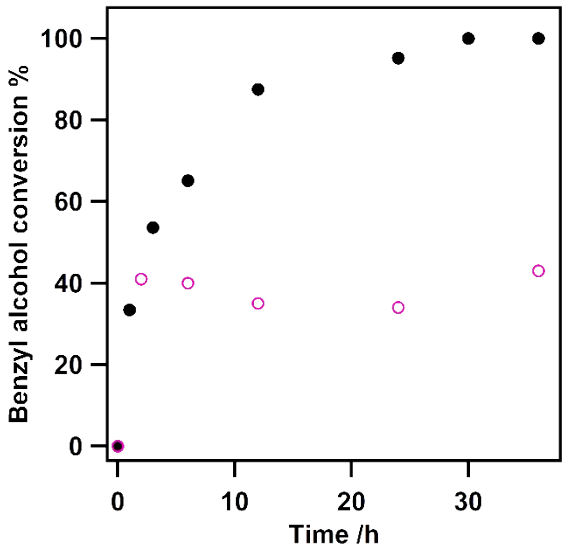

Fig. S11. Heterogeneity test for $Cu_{0.18}Ru_{0.05}CeO_z$. Black dots: Time-conversion plot of $Cu_{0.18}Ru_{0.05}CeO_z$. Pink dots: ammoxidation of benzyl alcohol after filtering and removing $Cu_{0.18}Ru_{0.05}CeO_z$ from the reaction. The benzyl alcohol conversion in the heterogeneity test was measured at 2, 6, 12, 24, and 36 h.

Reaction conditions: Benzyl alcohol (1.93 mmol), toluene (1.0 mL), dodecane (internal standard; 0.07 mL), 423 K. Mass balance was over 0.9. $Cu_{0.18}Ru_{0.05}CeO_z$ (74 mg), Ru/Cu/benzyl alcohol/NH_3/dodecane = 1/3.5/100/191/100.

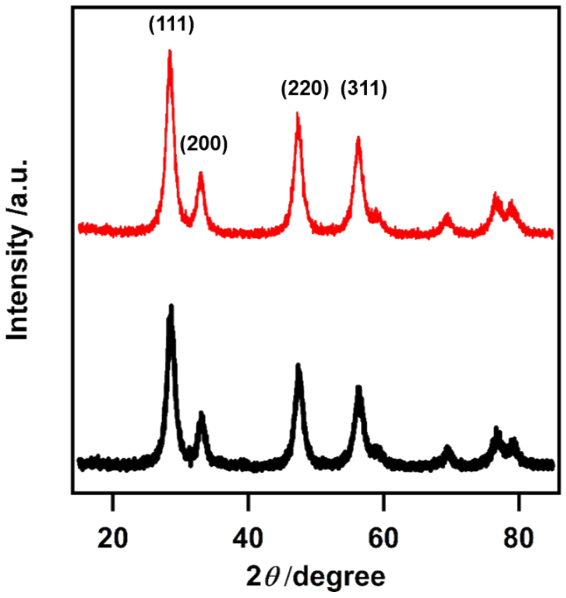

Fig. S12. XRD patterns of $Cu_{0.18}Ru_{0.05}CeO_z$ before and after the ammoxidation of benzyl alcohol for 24 h at 423 K. Black line: $Cu_{0.18}Ru_{0.05}CeO_z$ before the reaction. Red line: $Cu_{0.18}Ru_{0.05}CeO_z$ after the reaction.

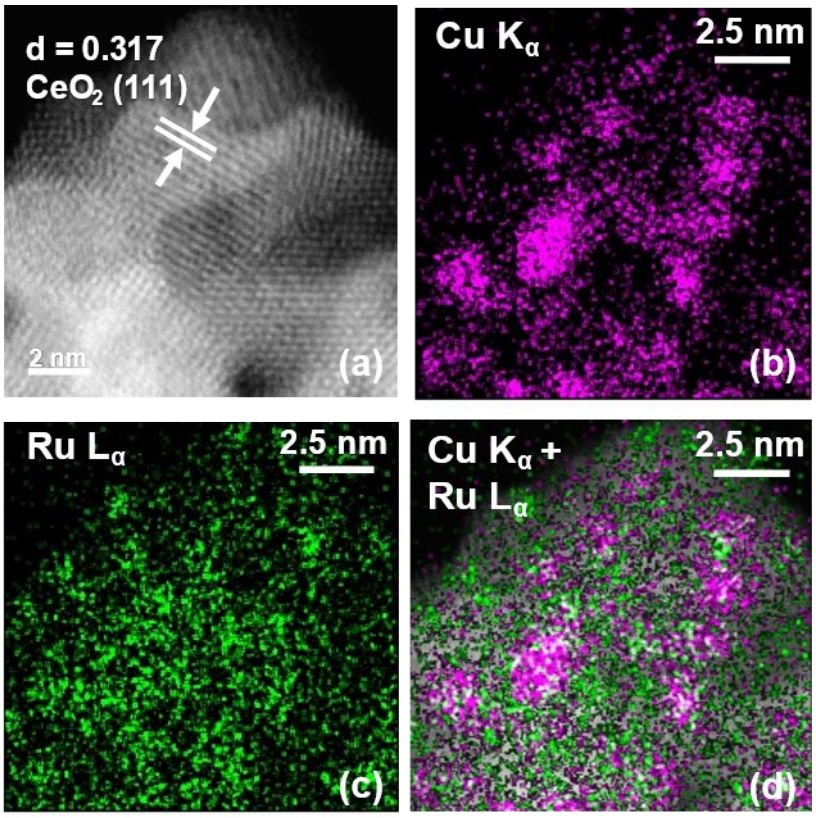

Fig. S13. (a) HAADF-STEM images of $Cu_{0.18}Ru_{0.05}CeO_z$ after the ammoxidation of benzyl alcohol for 24 h at 423 K, and (b) EDS map of Cu, (c) EDS map of Ru, and (d) overlapped EDS maps of Cu and Ru.

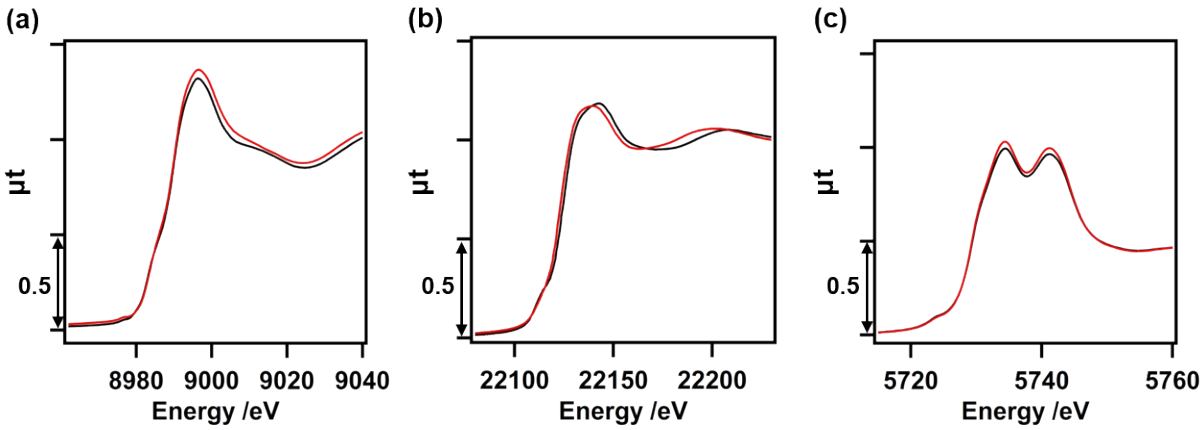

Fig. S14. (a) Cu K-edge, (b) Ru K-edge, and (c) Ce L_{III}-edge XANES spectra of $Cu_{0.18}Ru_{0.05}CeO_z$ after the ammoxidation of benzyl alcohol for 24 h at 423 K (with 0.32 MPa of NH_3 and 1.0 MPa of O_2). Black lines: XANES spectra of as-prepared $Cu_{0.18}Ru_{0.05}CeO_z$ before the reaction. Red lines: XANES spectra of $Cu_{0.18}Ru_{0.05}CeO_z$ after the ammoxidation of benzyl alcohol for 24 h at 423 K.

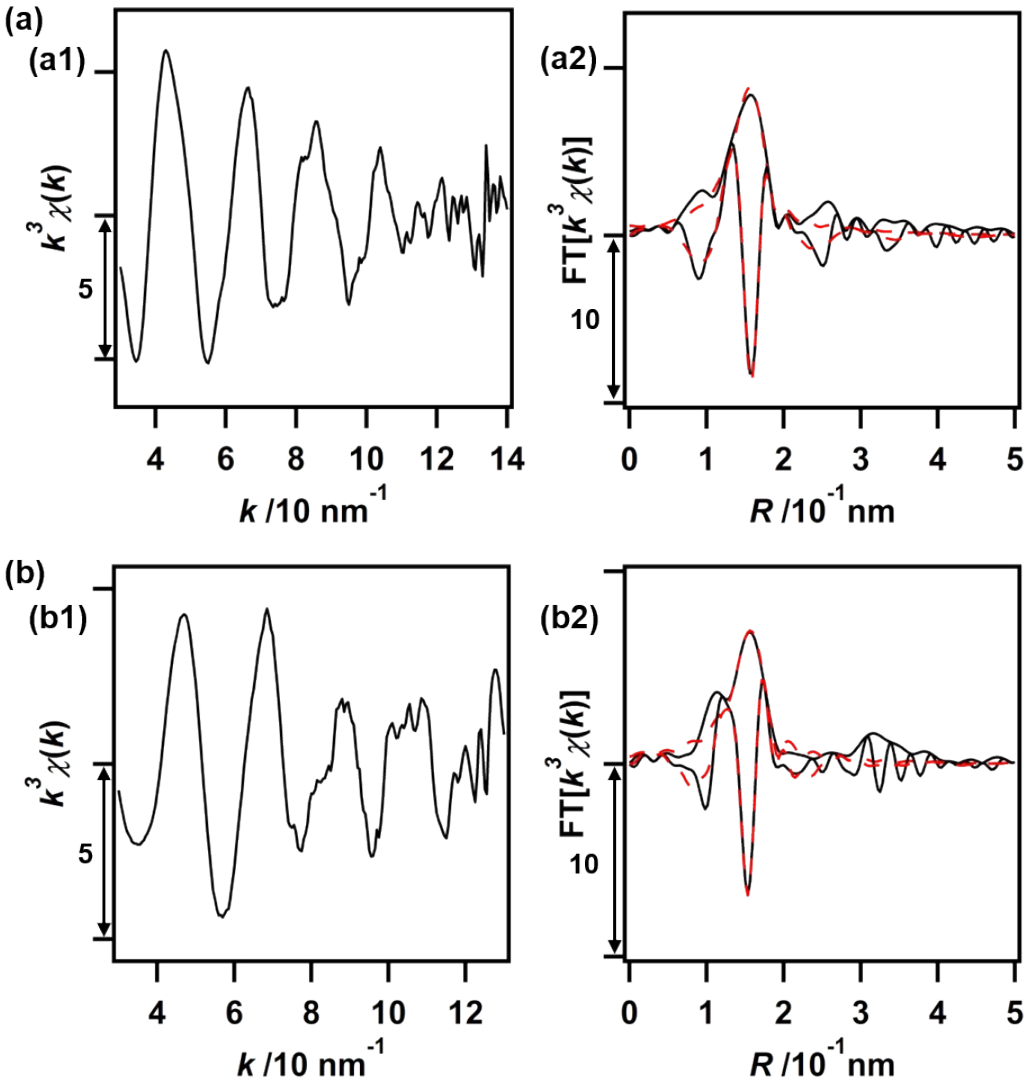

Fig. S15. (a) Cu K-edge EXAFS (a1) oscillations and (a2) Fourier transforms of $Cu_{0.18}Ru_{0.05}CeO_z$ after the ammoxidation of benzyl alcohol for 24 h at 423 K (k = 30–140 nm^{-1}). (b) Ru K-edge EXAFS (b1) oscillations and (b2) Fourier transforms of $Cu_{0.18}Ru_{0.05}CeO_z$ after the ammoxidation of benzyl alcohol for 24 h at 423 K (k = 30–130 nm^{-1}). In (a2) and (b2), black solid lines show the observed data and red dashed lines show the fitted data.

Table S14. Structural Parameters Obtained by the Curve-Fitting Analysis of Cu K-edge EXAFS Fourier Transform (Measured at 298 K) of $Cu_{0.18}Ru_{0.05}CeO_z$ After the Ammoxidation of Benzyl Alcohol for 24 h at 423 K

Sample	Shell	CN	R /nm	ΔE /eV	σ^2 /10^{-5} nm^2	R_f %
$Cu_{0.18}Ru_{0.05}CeO_z$ after reaction	Cu-O	5.5 ± 1.2	0.194 ± 0.002	2.0 ± 3.3	7 ± 2	0.6

S_0^2 was fixed as 0.70, k = 30–140 nm^{-1}, R = 0.12–0.19 nm.

Table S15. Structural Parameters Obtained by the Curve-Fitting Analysis of Ru K-edge EXAFS Fourier Transform (Measured at 298 K) of $Cu_{0.18}Ru_{0.05}CeO_z$ After the Ammoxidation of Benzyl Alcohol for 24 h at 423 K

Sample	Shell	CN	R /nm	ΔE /eV	σ^2 /10^{-5} nm^2	R_f %
$Cu_{0.18}Ru_{0.05}CeO_z$ after reaction	Ru-O	4.2 ± 1.5	0.203 ± 0.003	11 ± 5.4	6 ± 3	0.3

S_0^2 was fixed as 0.86, k = 30–130 nm^{-1}, R = 0.12–0.19 nm.

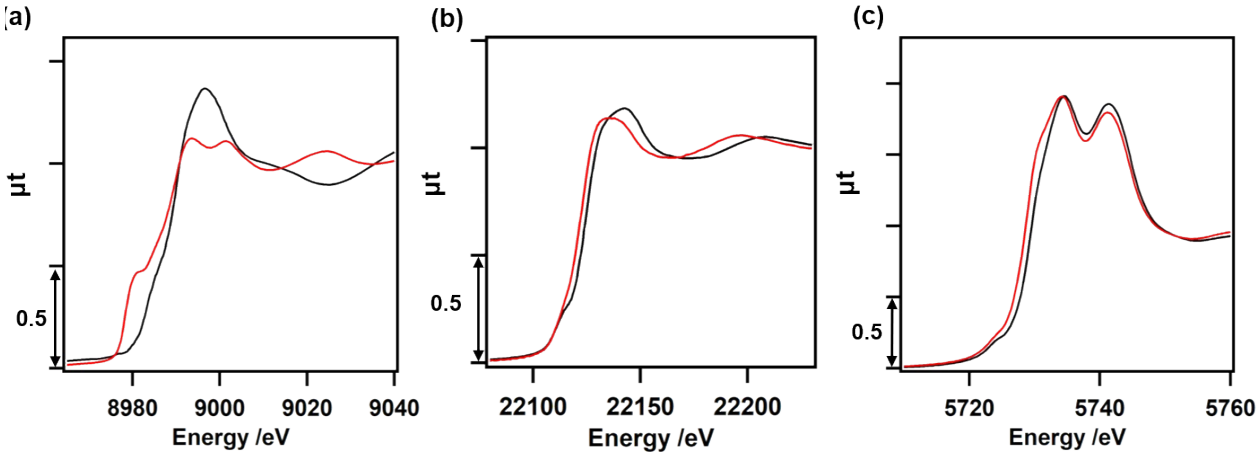

Fig. S16. (a) Cu K-edge, (b) Ru K-edge, and (c) Ce L_{III}-edge XANES spectra of $Cu_{0.18}Ru_{0.05}CeO_z$ before (black) and after (red) the ammoxidation of benzyl alcohol under an inert atmosphere for 24 h at 423 K (with 0.32 MPa of NH_3 and 1.0 MPa of N_2).

Table S16. Catalytic Performance of $Cu_{0.18}Ru_{0.05}CeO_z$ and the Control Groups for the Selective Oxidation of Benzyl Alcohol

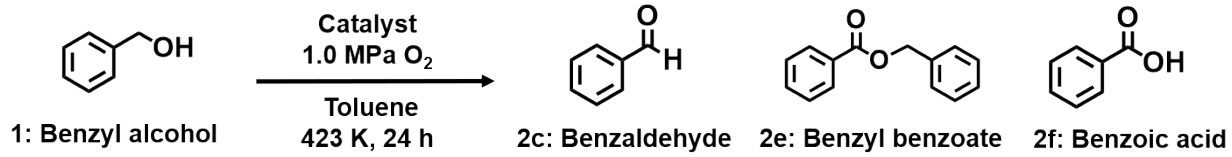

1: Benzyl alcohol | 2c: Benzaldehyde | 2e: Benzyl benzoate | 2f: Benzoic acid

Entry	Catalyst	Conversion of **1** %	Selectivity of **2c** %	Selectivity of **2e** %	Selectivity of **2f** %
1[a]	$Cu_{0.18}Ru_{0.05}CeO_z$	>99	5	14	78
2[b]	$Cu_{0.18}CeO_z$	30	81	38	0
3[c]	$Ru_{0.04}CeO_z$	>99	7	14	83
4[d]	CeO_z	26	80	0	0
5	Blank	0	0	0	0

Reaction conditions: **1** (1.93 mmol), toluene (1.0 mL), dodecane (0.07 mL), O_2 (1.0 MPa), 423 K, 24 h. Mass balance was over 0.9. [a]$Cu_{0.18}Ru_{0.05}CeO_z$ (74 mg), Ru/Cu/**1**/dodecane = 1/3.5/100/100. [b]$Cu_{0.18}CeO_z$ (77 mg), Cu/**1**/dodecane = 1/29/29. [c]$Ru_{0.04}CeO_z$ (72 mg), Ru/**1**/dodecane = 1/100/100. [d]CeO_z (74 mg), **1**/dodecane = 1/1.

Table S17. Catalytic Performance of $Cu_{0.18}Ru_{0.05}CeO_z$ and the Control Groups for the Ammoxidation of Benzaldehyde

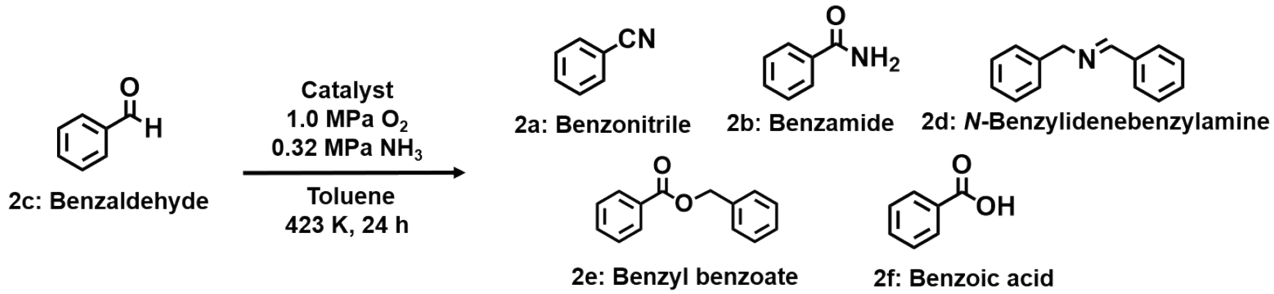

Entry	Catalyst	Conversion of **2c** %	Select. of **2a** %	Select. of **2b** %	Select. of **2d** %	Select. of **2e** %	Select. of **2f** %
1[a]	$Cu_{0.18}Ru_{0.05}CeO_z$	>99	91	9	0	0	0
2[b]	$Cu_{0.18}CeO_z$	>99	81	10	0	0	2
3[c]	$Ru_{0.04}CeO_z$	97	5	16	0	0	2
4[d]	CeO_z	97	2	18	0	1	0
5	None	>99	1	19	0	0	0

Reaction conditions: **2c** (1.96 mmol), toluene (1.0 mL), dodecane (0.07 mL), NH_3 (0.32 MPa), O_2 (1.0 MPa), 423 K, 24 h. Mass balance was over 0.9 except for entries 3, 4, and 5. [a]$Cu_{0.18}Ru_{0.05}CeO_z$ (74 mg), Ru/Cu/**2c**/NH_3/dodecane = 1/3.5/100/191/100. [b]$Cu_{0.18}CeO_z$ (77 mg), Cu/**2c**/NH_3/dodecane = 1/29/58/29. [c]$Ru_{0.04}CeO_z$ (72 mg), Ru/**2c**/NH_3/dodecane = 1/100/191/100. [d]CeO_z (74 mg), **2c**/NH_3/dodecane= 1/1.91/1.

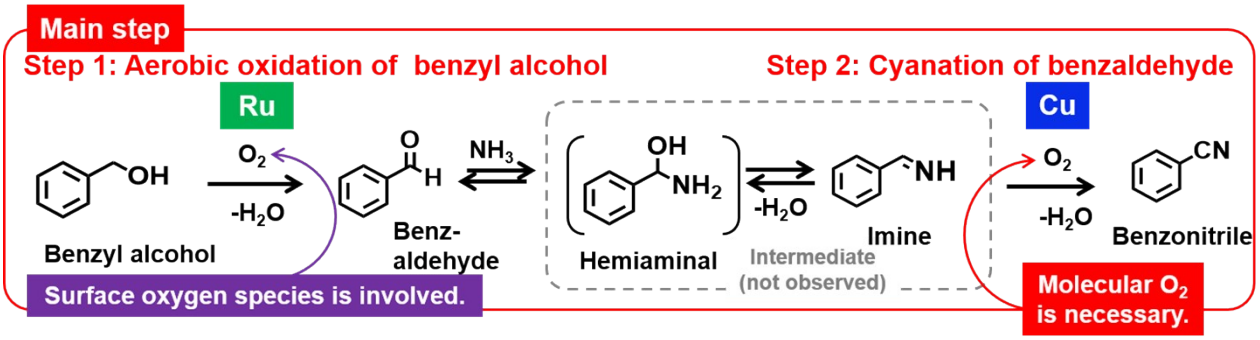

Scheme S1. Ammoxidation of benzyl alcohol and the roles of Cu and Ru species in each reaction step.

General setup for the experiments

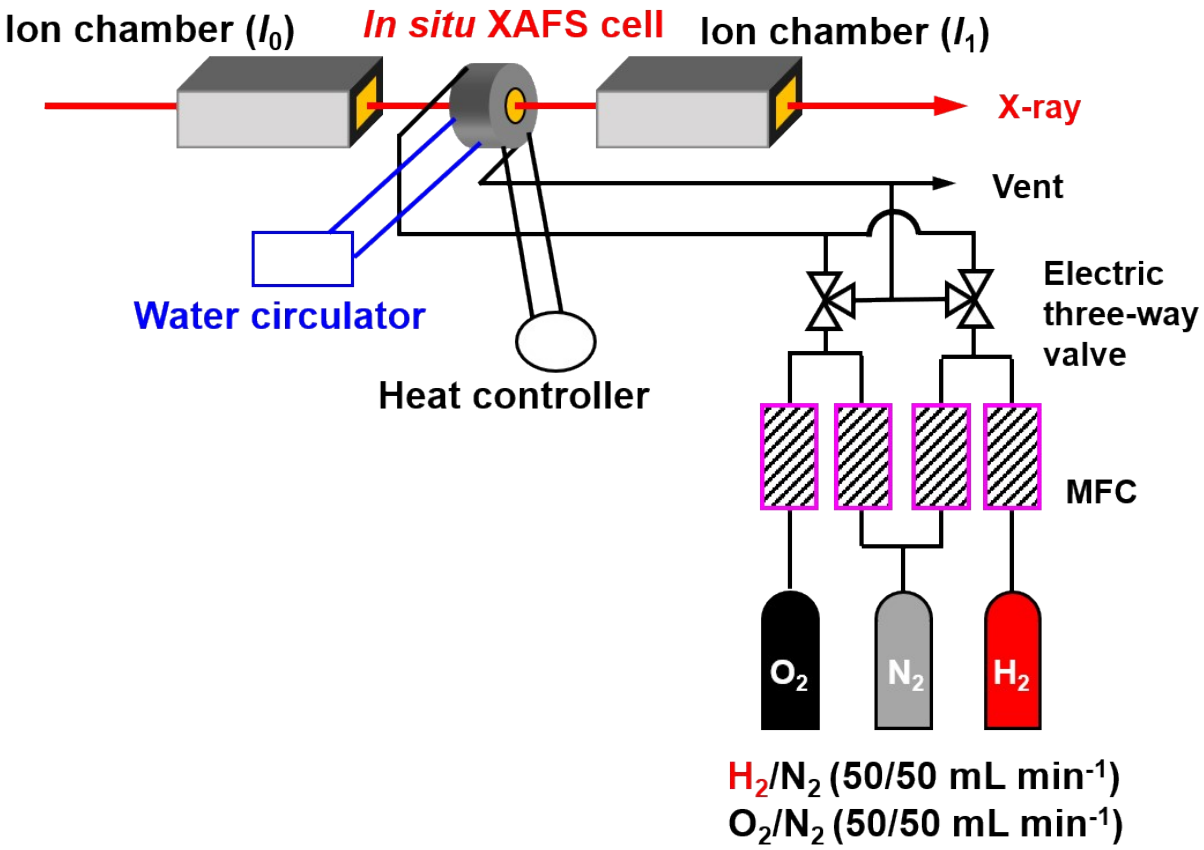

Fig. S17. Setup for *in situ* QXAFS measurements for H_2 reduction and O_2 oxidation.

References:

(1) D. R. Mullins, *Surf. Sci. Rep.,* 2015, **70**, 42–85.

(2) G. Yan, Y. Tang, Y. Li, L. Nguyen, T. Sakata, K. Higashi, F. F. Tao and P. Sautet, *Nat. Catal.* 2022, **5**, 119–127.

(3) S. Ikemoto, X. Huang, S. Muratsugu, S. Nagase, T. Koitaya, H. Matsui, G. Yokota, T. Sudoh, A. Hashimoto, Y. Tan, S. Yamamoto, J. Tang, I. Matsuda, J. Yoshinobu, T. Yokoyama, S. Kusaka, R. Matsuda and M. Tada, *Phys. Chem. Chem. Phys.*, 2019, **21**, 20868–20877.

(4) Z. Li, K. Werner, K. Qian, R. You, A. Płucienik, A. Jia, L. Wu, L. Zhang, H. Pan, H. Kuhlenbeck, S. Shaikhutdinov, W. Huang and H. J. Freund, *Angew. Chem., Int. Ed.*, 2019, **58**, 14686–14693.

(5) C. Yang, X. Yu, S. Heißler, A. Nefedov, S. Colussi, J. Llorca, A. Trovarelli, Y. Wang and C. Wöll, *Angew. Chem., Int. Ed.*, 2017, **56**, 375–379.